Magnetotelluric imaging beneath the Taiwan orogen: An arc-continent collision

Edward A. Bertrand,[1,2] Martyn J. Unsworth,[3] Chih-Wen Chiang,[4,5] Chow-Son Chen,[6] Chien-Chih Chen,[6] Francis T. Wu,[7] Ersan Türkoğlu,[3,8] Han-Lun Hsu,[6] and Graham J. Hill[1]

Received 20 July 2011; revised 29 October 2011; accepted 3 November 2011; published 7 January 2012.

[1] The Taiwan orogen has formed since the late Miocene by oblique collision between the Luzon Volcanic Arc on the Philippine Sea Plate, and the Eurasian continental margin. This oblique collision has produced an orogen that decreases in age from north to south, and permits study of the temporal evolution of an arc-continent collision. These factors make Taiwan a favorable location to study the process of arc-continent collision. The first long-period magnetotelluric (MT) measurements were recorded in Taiwan as part of the Taiwan Integrated Geodynamics Research (TAIGER) project in 2006–7. Measurements were made at 82 sites on three transects across south, central and north Taiwan, that span the breadth of the orogen and cross all major tectonic boundaries. Robust, remote reference processing of the MT time series data resulted in high-quality soundings that were modeled in both 2 and 3-dimensions. These MT models support predictions of lithospheric deformation (i.e., thick-skinned tectonics) beneath the Central Ranges in south and central Taiwan, but are inconsistent with predictions of orogen-scale thin-skinned models. The MT resistivity model for northern Taiwan is consistent with dewatering of the subducting Philippine slab, and with deformation described by the subducting-indenter tectonic model. Modeling the TAIGER MT data has definitively shown that conductive, and seismically active crustal structures, exist to 30+ km beneath the orogen. These conductive regions, interpreted as interconnected fluid, map pervasive zones of collisional deformation that are lithospheric in scale.

Citation: Bertrand, E. A., M. J. Unsworth, C.-W. Chiang, C.-S. Chen, C.-C. Chen, F. T. Wu, E. Türkoğlu, H.-L. Hsu, and G. J. Hill (2012), Magnetotelluric imaging beneath the Taiwan orogen: An arc-continent collision, *J. Geophys. Res.*, *117*, B01402, doi:10.1029/2011JB008688.

1. Introduction

[2] Arc-continent collisions have occurred since the Archean and cause deformation of the continents, control the distribution of natural resources, and also cause natural hazards from associated earthquakes and landslides [*Okaya et al.*, 2007]. However, the study of these collisions in ancient orogens is hindered by erosion and post-orogenic tectonic overprinting. Thus, studies of active collisions are required for detailed and well constrained analysis of the mechanics of mountain building and associated deformation processes [*Malavieille et al.*, 2002].

[3] At present, active arc-continent collisions are occurring in East Timor, Papua New Guinea, and Taiwan [*Huang et al.*, 2000]. Several key factors combine to make Taiwan a favorable location to study an active arc-continent collision and include: (1) Since first recognition of Taiwan as an arc-continent collision [*Chai*, 1972], extensive research has established the overall geologic framework and plate tectonic kinematics. (2) The high rate of plate convergence (82 mm/yr along an azimuth of N54°W) [*Yu et al.*, 1997] coupled with the sub-tropical climate produces one of the most rapidly evolving locations on Earth. The resulting steep topography and deeply incised valleys expose high-grade metamorphic rocks in the hinterland. (3) Oblique convergence between the Luzon Volcanic Arc (LVA) on the Philippine Sea Plate (PSP) and the Eurasian Plate (EUP) margin has developed a young orogen that displays the entire evolution of an arc-continent collision, from initiation to collapse [*Shyu et al.*, 2005]. Taiwan now occupies a pivotal position on the boundary of the Eurasian and Philippine Sea Plates (Figure 1a). Offshore southern Taiwan, subduction of oceanic lithosphere results in the formation of a submarine accretionary prism and an active magmatic arc [*Yu et al.*,

[1]GNS Science, Lower Hutt, New Zealand.
[2]Formerly at Department of Physics, University of Alberta, Edmonton, Alberta, Canada.
[3]Department of Physics, University of Alberta, Edmonton, Alberta, Canada.
[4]Department of Geosciences, National Taiwan University, Taipei, Taiwan.
[5]Formerly at Institute of Geophysics, National Central University, Jhongli, Taiwan.
[6]Institute of Geophysics, National Central University, Jhongli, Taiwan.
[7]Department of Geological Sciences and Environmental Studies, State University of New York at Binghamton, Binghamton, New York, USA.
[8]Now at Quantec Geoscience, Toronto, Ontario, Canada.

0148-0227/12/2011JB008688

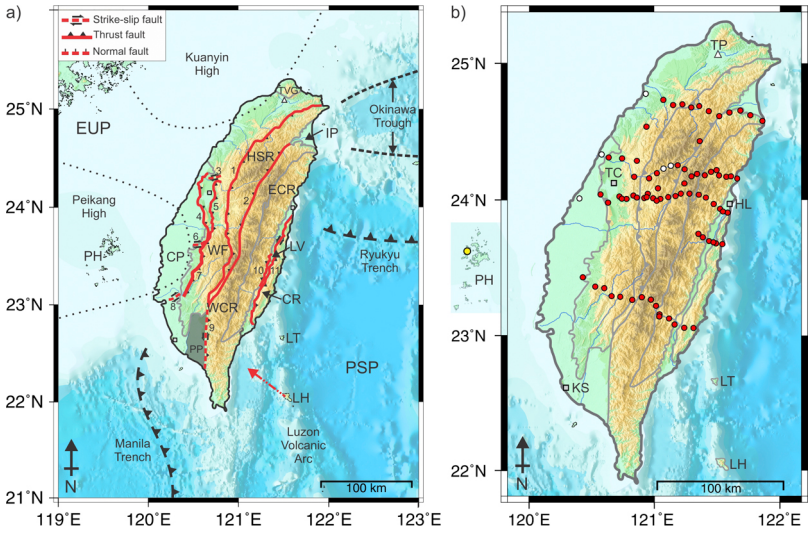

Figure 1. (a) Geologic and tectonic map of Taiwan and the surrounding region. Main geological provinces are abbreviated as follows: CP, Coastal Plain; WF, Western Foothills; HSR, Hseuhshan Range; W/ECR, Western/Eastern Central Range; LV, Longitudinal Valley; CR, Coastal Range; and IP, Ilan Plain. Major faults are numbered as follows: 1, Chuchih Fault; 2, Lishan Fault; 3, Tuntzuchiao Fault; 4, Changhua Fault; 5, Chelungpu Fault; 6, Meishan Fault; 7, Chukou Fault; 8, Hsinhua Fault; 9, Chaochou Fault; 10, Central Range Fault; 11, Longitudinal Valley Fault (based on *Shyu et al.* [2005] and *Ng et al.* [2009]). Relative convergence between the PSP and EUP is indicated by the red dashed arrow (82 mm/yr, N54°W) [*Yu et al.*, 1997]. Subduction trenches are abbreviated as follows: MT, Manila Trench; RT, Ryukyu Trench. Islands are abbreviated as follows: PH, Penghu Archipelago; LT, Lutao; LH, Lanhsu. PP, Pingtung Plain; TVG, Tatun Volcanic Group. Dashed lines delineate estimated boundaries of the Peikang and Kuanyin basement highs [*Mouthereau et al.*, 2002]. (b) Location map of 82 long-period magnetotelluric data measurements (red circles) in Taiwan. White circles indicate where only magnetic fields were recorded. Yellow circle denotes the remote reference station on the Penghu archipelago (PH). Major cities in Taiwan are abbreviated as follows: TP, Taipei; TC, Taichung; HL, Hualien; KS, Kaohsiung.

1999]. Onshore southern Taiwan, the emerging mountain belt reflects the transition from subduction to collision as the arc encroaches onto the continental margin. In contrast, post-collision collapse and extension occur progressively northward of 23.7°N as the orogen transfers to a region of back-arc extension [*Bos et al.*, 2003], and the subducting PSP contacts the EUP at depth [*Wu et al.*, 2009]. In central Taiwan, where collision began ~3 Ma [*Teng*, 1990], recent thermochronology [*Fuller et al.*, 2002] confirms earlier predictions that the orogen has reached a steady state, where uplift is balanced by erosion [*Suppe*, 1981]. Taiwan thus provides an ideal natural laboratory to study the time-evolution of processes involved in arc-continent collision from beginning to end.

[4] In 2004, an international study of the Taiwan arc-continent collision was initiated. The TAIGER (Taiwan Integrated Geodynamics Research) project was designed to collect the lithospheric-scale high-resolution data set required to distinguish between debated end-member tectonic models of central Taiwan (1. thin-skinned tectonics [*Suppe*, 1987]; 2. thick-skinned lithospheric deformation [*Wu et al.*, 1997]), and to investigate fundamental processes of arc-continent collisions. In 2006–2007, the first long-period magnetotellurics (MT) data were recorded at 82 sites across Taiwan as part of TAIGER (Figure 1b). Measurements were made on cross-island transects in south, central and north Taiwan to study the temporal evolution of the orogen.

[5] MT is a passive geophysical imaging technique that measures time variations of natural electromagnetic (EM) fields at the surface of the Earth. Measurements of these fields are used to generate inversion models of subsurface electrical resistivity as a function of depth [*Simpson and Bahr*, 2005]. The electrical resistivity models are interpreted and used to infer geological and rheological properties of interest. For example, in active tectonic environments, aqueous fluids or partial melt are the most likely contributors to large-scale zones of low resistivity [*Jiracek et al.*, 2007]. Thus, lithospheric scale MT models of the active arc-continent collision in Taiwan effectively map fluids and/or melts, which can dramatically lower the strength of crustal and upper mantle materials [*Cox*, 2005; *Rosenberg and Handy*, 2005]. Such low resistivity anomalies may therefore indicate mechanically weak zones where deformation is localized [*Wannamaker et al.*, 2008]. Since MT is the only EM exploration technique capable of imaging to depths greater than 10 km [*Unsworth*, 1999], and is very sensitive to the presence of minor constituents that can profoundly influence crustal rheology [*Karato and Wenk*, 2002], MT has proven to be a valuable addition to lithospheric scale studies of convergent margins.

[6] Previously, subsets of the TAIGER MT data analyzed in 2-D have been shown to support the thick-skinned lithospheric deformation model for both southern [*Chiang et al.*, 2010] and central Taiwan [*Bertrand et al.*, 2009]. In this paper, the southern and central 2-D MT models are jointly

interpreted, and along-strike differences in resistivity structures are explained in terms of the northward age-progression of mountain building processes in Taiwan. In addition, the northern TAIGER MT data are presented and analyzed for the first time. The northern 2-D MT model is interpreted with reference to the subducting-indenter tectonic model [*Wu et al.*, 2009] that describes contact between the EUP and PSP to occur at increasing depth north of 23.7°N. Throughout Taiwan, low-resistivity structures in the TAIGER MT models map the locations of fluids, and show that collisional deformation is lithospheric in scale. Note that initial 3-D models of the TAIGER MT profiles are shown that yield very similar structures to the corresponding 2-D results, and justify the detailed 2-D interpretation presented in this paper. Detailed 3-D analysis of these MT data will form a future publication.

2. The Taiwan Arc-Continent Collision

[7] The island of Taiwan is located in a region whose geological structure and history has been controlled by the interactions of the Philippine Sea Plate and the Eurasian Plate. Taiwan is currently bracketed by subduction zones of opposite polarity (Figure 1a). Offshore southern Taiwan, the Eurasian oceanic lithosphere subducts eastward beneath the PSP along the Manila trench. Northeast of Taiwan, the PSP subducts northward beneath the EUP at the Ryukyu trench. Back-arc extension has formed the Okinawa trough, which extends into northern Taiwan as the Ilan Plain. In between these two subduction zones, Eurasian continental lithosphere (that is too buoyant to subduct) has collided with the LVA and formed the Taiwan orogen since the late Miocene. This collision is oblique and has resulted in an orogen that becomes progressively older from south to north Taiwan [*Byrne and Liu*, 2002].

2.1. Geological Provinces and Major Tectonic Features of Taiwan

[8] Eight primary geological provinces have been formed by the arc-continent collision and are oriented mainly parallel to the island long-axis (Figure 1a). In general, the Longitudinal Valley separates rocks of EUP affinity to the west from the accreted LVA rocks on the PSP to the east. The sub-units of EUP affinity are bounded mainly by faults (Figure 1a), and generally increase in age and metamorphic grade to the east [*Ernst et al.*, 1985].

[9] The westernmost, Coastal Plain (CP) consists of sedimentary deposits derived from the mountain ranges to the east [*Hickman et al.*, 2002]. These basin sediments unconformably overlie basement rocks of the Eurasian continental margin, which regionally dip to the east from flexure and downwarping in response to orogenic loading by the Taiwan hinterland [*Chou and Yu*, 2002]. To the east, The Western Foothills (WF) province comprises shallow marine to shelf clastic sediments [*Teng*, 1990] that are essentially unmetamorphosed and imbricated along numerous active folds and thrust faults trending mainly north or northeast and dipping east or southeast [*Tillman and Byrne*, 1995; *Yu et al.*, 1997]. The Western Foothills province is considered a classic example of a fold-and-thrust belt that is explained by thin-skinned tectonic models [*Suppe*, 1980; *Clark et al.*, 1993; *Twiss and Moores*, 2007]. The basal décollement [*Chapple*, 1978] beneath the WF of Taiwan dips moderately ($\beta = 6°$) within the upper crust and is well defined by extensive drilling, seismic reflection profiling and detailed surface mapping [*Suppe*, 1980, 1981, 1987].

[10] The east-dipping Chuchih Thrust Fault bounds the WF from the Taiwan slate belt, which comprises the Hseuhshan Range (HSR) and the Western Central Range (WCR) that are separated by the Lishan Fault. These provinces exhibit structural variations and differ in age and lithology, suggesting deposition in distinct structural settings on the Eurasian passive margin. Specifically, the HSR consists of Eocene-Oligocene shallow marine successions, metamorphosed at prehnite-pumpellyite facies in the west and increasing to lower greenschist facies in the east [*Clark et al.*, 1993; *Fisher et al.*, 2002; *Gourley et al.*, 2007]. In comparison, the WCR rocks are finer grained and inferred to have been deposited closer to the continental slope than those in the HSR [*Wu et al.*, 1997]. The thick Oligocene strata of the HSR are not present in the WCR, which consists of only Eocene and Miocene slates and minor interbedded sandstones with southeast dipping structural fabric [*Fisher et al.*, 2002, 2007]. Structural studies suggest that the HSR formed as a regional-scale pop-up structure, bounded by steeply dipping thrust faults [*Fisher et al.*, 2007]. The eastern boundary is marked by the steep, west-dipping Lishan Fault, which is now widely accepted to be an inverted passive margin growth fault, initially formed during Oligocene rifting of the Eurasian margin [*Clark et al.*, 1993; *Fisher et al.*, 2002; *McIntosh et al.*, 2005]. The Lishan Fault is a major structural boundary and highlights the importance of pre-existing features in the development of the orogen [*Gourley et al.*, 2007]. East of the slate belt are the exposed pre-Tertiary metamorphic rocks of the Eastern Central Range (ECR). The ECR consists of a complex of high grade, multideformed schists, gneisses and some marble that have been exposed after deep (>10 km) burial [*Wu et al.*, 1997]. The ECR exposes rocks of the highest metamorphic grade in the orogen, and defines the eastern boundary of rocks with EUP affinity.

[11] The narrow, NNE trending Longitudinal Valley (LV) is a fault-bounded depression filled with 1–2 km of coarse, clastic sediments [*Tsai et al.*, 1974] that overlies the suture zone between the PSP and the EUP [*Yu and Kuo*, 2001; *Hickman et al.*, 2002]. East of the LVF lies the Coastal Range (CR) comprising the remnant telescoped Luzon Volcanic Arc and forearc basin that have collided with and accreted to the Eurasian continental margin [*Barrier and Angelier*, 1986]. In northeastern Taiwan, the Ilan Plain (IP) represents the onshore extension of the Okinawa Trough; the back-arc basin associated with subduction at the Ryukyu trench [*Teng*, 1996].

2.2. Tectonic Models

[12] Several models have been proposed to explain the tectonics that give rise to the topography and geology observed across the Taiwan orogen. Of importance to these models is identification of the Ryukyu subduction zone offshore Eastern Taiwan. A recent detailed investigation used seismicity and 3-D seismic velocity structure to locate the western terminus of the Ryukyu trench at 23.7°N, beneath the Coastal Range [*Wu et al.*, 2009]. South of 23.7°N, major disagreement between existing tectonic models is focused on

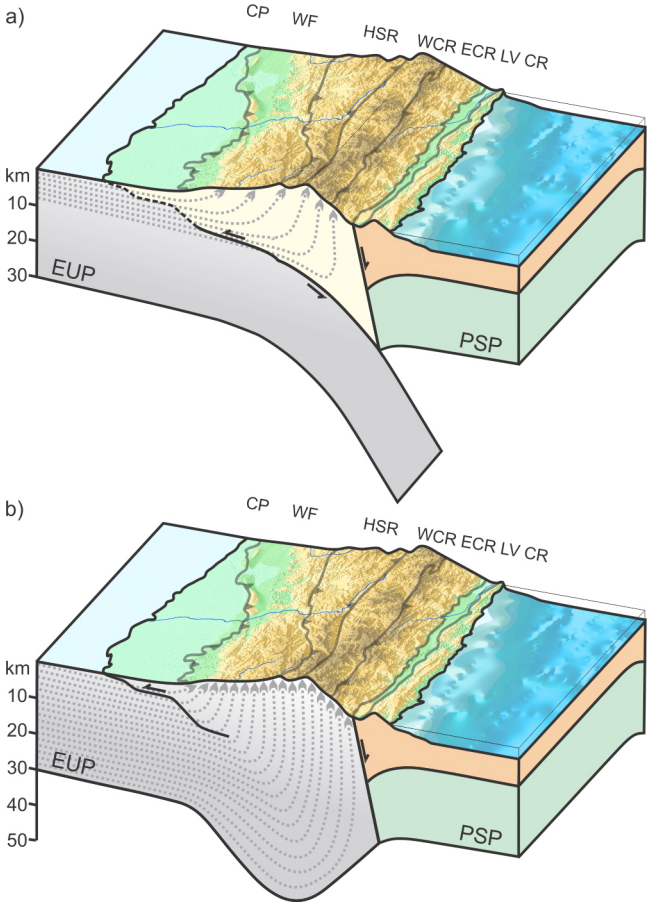

Figure 2. (a) Schematic of the thin-skinned tectonic model. (b) Schematic of the thick-skinned lithospheric deformation model. Vertical exaggeration is ~1.5× and particle paths are drawn assuming a fixed PSP reference frame.

whether collision of the LVA with the Eurasian continental margin permitted continued subduction of the Eurasian continental lithosphere during orogen formation. This difference divides the numerous models proposed into two end-members: (1) thin-skinned tectonics (Figure 2a) [*Suppe*, 1987], which predicts a detachment within the upper crust, below which subduction of the undeformed continental lithosphere occurs, and (2) thick-skinned lithospheric deformation (Figure 2b) [*Wu et al.*, 1997], which infers vertically continuous deformation of the entire crust and upper mantle, resulting in a thickened crustal root.

[13] The two end-member tectonic models agree on the structures present beneath western Taiwan (i.e., west of the slate belt), but predict different structures at mid and lower crustal depths beneath the Central Ranges. Past debate over these models has not yet been resolved for two main reasons: (1) both models satisfactorily explain the surface geology and morphology of the Taiwan orogen, and (2) until recently, insufficient geophysical data were available to unequivocally resolve the deep crustal structure beneath the Central Ranges.

[14] For example, while most earthquake relocation models indicate an aseismic region beneath the WCR, and clusters of deep-crustal seismicity [e.g., *Wu et al.*, 2004; *Gourley et al.*, 2007; *Wu et al.*, 2008], a seismically defined upper-crustal sub-horizontal décollement was interpreted by *Carena et al.* [2002] beneath the Central Ranges. Partly contributing to this discrepancy is the difficulty in relocating events beneath a narrow island [*Gourley et al.*, 2007].

[15] In reality, the correct model is likely to be a combination of these end-members, and additionally could vary with location along the orogen strike as inferred by *McIntosh et al.* [2005]. Inherent uncertainties present in any individual geophysical technique require that a detailed multidisciplinary approach be undertaken to unambiguously resolve the deep crustal structure beneath the Taiwan orogen.

3. Acquisition and Dimensionality of TAIGER MT Data

[16] The TAIGER project collected long-period (0.1 < period < 10000 s) MT data on multiple land-based transects across Taiwan to yield models of electrical resistivity and provide constraints on the lithospheric composition and strength beneath the orogen. Since differences in the lithospheric structure between the end-member tectonic models were expected to be the greatest in central Taiwan, there was a particular need to collect high quality deep sounding MT data in this region. In total, 82 long-period MT measurements were made, mainly on transects crossing south, central and northern Taiwan (Figure 1b) using 15 NIMS (Narod Intelligent Magnetotelluric Systems) instruments owned by the University of Alberta. These data were collected during two separate field campaigns in Fall 2006 and Spring 2007, in joint fieldwork by the University of Alberta and National Central University. To reduce the effect of high levels of cultural EM noise on the densely populated island, a remote reference station [*Gamble et al.*, 1979] was operated on the Penghu archipelago during measurements on the island proper. MT data processed using a remote reference and collected away from obvious sources of noise (power lines, highways, etc.) resulted in high quality soundings.

[17] Prior to modeling, careful dimensionality analysis must be completed to determine if a 1-D, 2-D or 3-D interpretation is needed. Simplified analysis of MT data in dimensions lower than required can lead to artifacts in inversion models and erroneous interpretations [*Simpson and Bahr*, 2005]. Most often a 1-D approach is insufficient, and MT data are routinely modeled using a 2-D approximation. For MT data that display overall 2-D characteristics despite some 3-D effects, results obtained using 2-D inversion algorithms can be valid [*Wannamaker*, 1999; *Ledo*, 2005]. In Taiwan, geologic structures are largely 2-D and generally parallel the island long-axis with length scales nearly four-times their cross-island extent [*Yen et al.*, 1998]. However, the island of Taiwan is located in a region of complex tectonics and is surrounded by seawater of variable depths (Figure 1a). These factors will contribute to 3-D induction and require careful data analysis to determine if overall 2-D behavior persists, or if 3-D interpretation is needed. As described in detail by *Bertrand et al.* [2009] and *Chiang et al.* [2010], the TAIGER MT data collected in central and southern Taiwan possess an overall 2-D

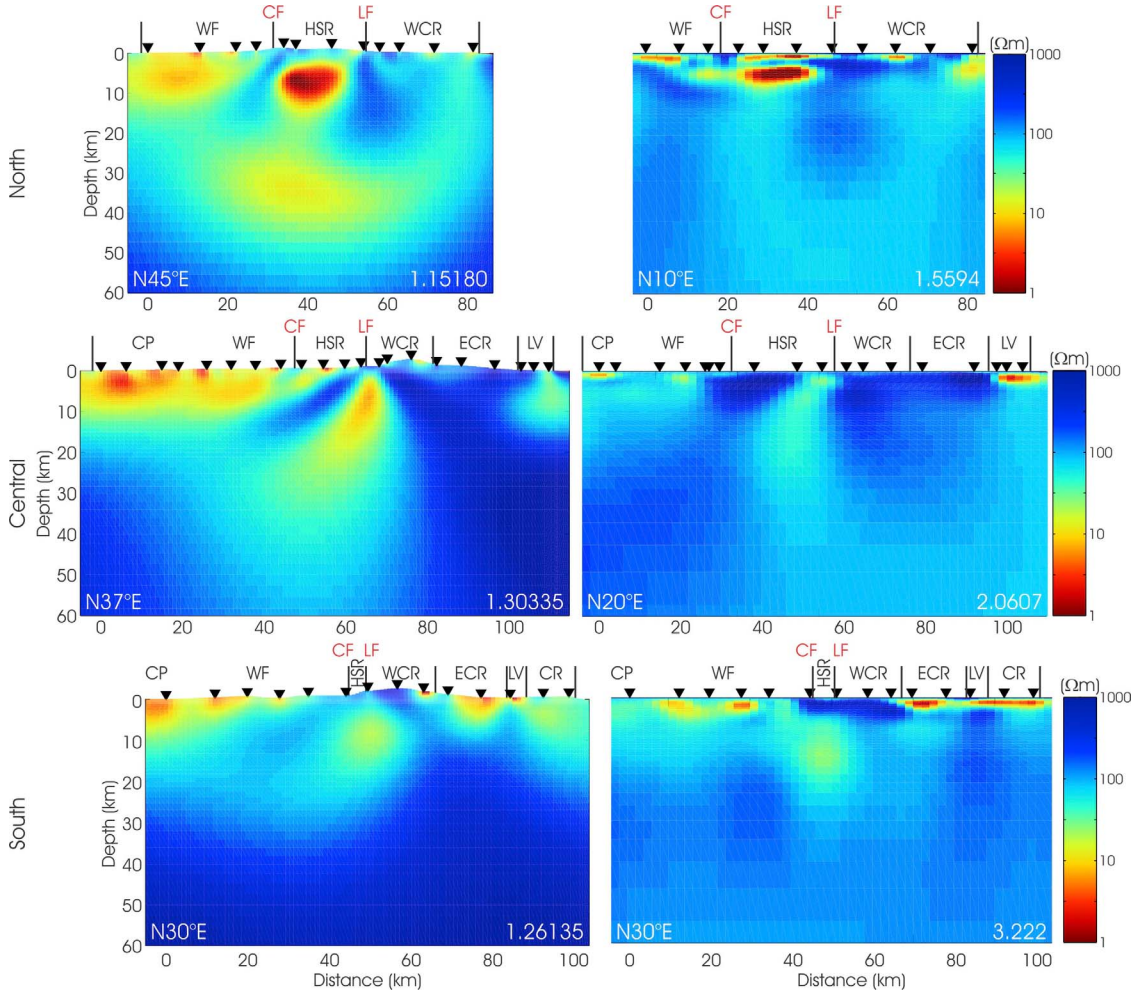

Figure 3. (left) The 2-D inversion models of the TE, TM, and tipper data for north, central, and south Taiwan. (right) The 3-D inversion models of the full MT impedance tensor data. The orientation of each profile is shown in the bottom left corner of each model, and the r.m.s. data misfit is indicated in the bottom right corner. Models are aligned to the Lishan Fault.

behavior. Figures S1–S4 in the auxiliary material summarize the dimensionality analysis of the TAIGER MT data (including the northern profile MT data), and justifies detailed modeling in 2-dimensions.[1]

[18] However, to unequivocally ensure that resistivity features in the 2-D models are robust, these same MT data were also inverted using the 3-D inversion algorithm, WS3DINVMT [*Siripunvaraporn et al.*, 2005]. Figure 3 shows strong similarity between structures observed in corresponding 2-D and 3-D models and justifies the detailed 2-D analysis carried out in this paper. Note that despite similar structures present in the 2-D and 3-D models, the depth extent and the absolute resistivity of equivalent features is variable. However, the key observation is that the resistivity structures themselves are similar in both the 2-D and 3-D models. The 3-D models are not used for detailed interpretation since the intensive computation requirements forces modeling with a reduced data set and on a coarse mesh, yielding lower resolution in comparison to the 2-D models (see the auxiliary material for more information).

4. Orogenic Evolution: Southern and Central Taiwan

[19] The southern and central TAIGER MT data have been shown to provide strong evidence for the occurrence of thick-skinned tectonics beneath the Central Ranges [*Bertrand et al.*, 2009; *Chiang et al.*, 2010]. Here, resistivity models of southern and central Taiwan are presented in unison. In addition, detailed quantitative comparison between the southern MT model and a corresponding tomographic P wave velocity model is shown, and displayed adjacent to an identical comparison that was previously reported for the central TAIGER data [*Bertrand et al.*, 2009]. Along-strike variations in the MT resistivity models are explained in terms of the orogenic evolution from south to central Taiwan.

4.1. The 2-D MT Inversion

[20] In central Taiwan, 47 stations were deployed on two closely spaced parallel transects (Figure 1b). While these

[1]Auxiliary materials are available in the HTML. doi:10.1029/2011JB008688.

data indicate an overall 2-D geoelectric structure, careful data analysis was undertaken to select a subset of 21 high-quality MT stations that showed a minimum 3-D behavior [*Bertrand et al.*, 2009]. In southern Taiwan, 14 MT measurements were made that show a consistent 2-D geoelectric strike direction that is parallel to the orogen structure and coast [*Chiang et al.*, 2010]. However, the 6 westernmost MT stations recorded anomalous TM mode phase values that exceed 90° at periods greater than 100 s. Since out-of-quadrant phase data cannot be explained by a 2-D resistivity model [*Ichihara and Mogi*, 2009] these TM mode data were not included in subsequent MT models of southern Taiwan.

[21] The NLCG6 2-D inversion algorithm of *Rodi and Mackie* [2001] was used to generate smooth resistivity models of the MT data collected in southern and central Taiwan. Error floors of 20%, 2.2° and 0.03 were used for the apparent resistivity, phase and tipper data, respectively. Unlike the phase, the apparent resistivity data are susceptible to galvanic distortion. However, setting a large error floor for the resistivity down-weights these effects and mitigates any distortion present [*Li et al.*, 2003]. In addition, inversion models included the known topography and bathymetry along the profile (Figure S5), and the algorithm was set to solve for the static shift coefficients at each site during late-stage iterations. Many inversion models were computed for a range of control parameters and from a variety of starting models to ensure that significant resistivity features are robust and required by these MT data (see Figures S6–S8 in the auxiliary material for more details). Final inversions of the impedance and induction vector data produced resistivity models that fit the measurements to within an acceptable r.m.s. misfit of 1.261 for southern Taiwan (Figure 4a) and 1.304 for central Taiwan (Figure 4b).

4.2. Resistivity Model Interpretation

[22] The 2-D inversion models of southern (Figure 4a) and central (Figure 4b) Taiwan show strong similarity. Namely, low resistivity occurs in the foreland basin (FBC), the Central Ranges are resistive (except for a near-surface conductor beneath the ECR in southern Taiwan (HFC) that has been associated with localized hydrothermal fluids [*Chiang et al.*, 2010]) and a conductor occurs beneath the Lishan Fault (LFC) in the upper to middle crust. Given this similarity, it is reasonable to propose that the same style of tectonics (i.e., thick-skinned lithospheric deformation) occurs at both latitudes. However, two key elements of the LFC were rigorously tested in central Taiwan [*Bertrand et al.*, 2009] to provide strong evidence for the thick-skinned tectonic model. These key points include: (1) Quantitative correlation of the resistivity model with a tomographic P wave velocity model showed that a few percent saline aqueous fluids could explain the observed conductivity of the LFC. (2) Constrained inversions were computed with a resistive basement fixed at depths of 10, 20 and 30 km. Observation of (a) the tipper anomaly at sites adjacent the Lishan Fault, (b) the integrated conductivity (conductance) beneath the profile, and (c) the reduction in r.m.s. misfit for these constrained inversions, were used to show that the LFC extended beyond a depth of 10 km; the inferred level of the thin-skinned décollement in central Taiwan [*Carena et al.*, 2002]. Note that if a décollement were present, it might be expected to disrupt upward fluid migration [*Bertrand et al.*, 2009]. Therefore, these same procedures are carried out here to test whether quantitative evidence exists in the southern MT data to support the thick-skinned lithospheric deformation model.

4.3. Correlation of Resistivity and Seismic Velocity

[23] As performed for the central Taiwan MT data (Figures 4b, 4d, 4f, and 4h) [*Bertrand et al.*, 2009], the resistivity model of southern Taiwan was compared with a tomographic model of P wave velocity estimates on an x = y = 5, z = 2 km grid that include first arrival data from the TAIGER active seismic transects collected in 2007–8. Visual inspection of these models (Figures 4a and 4c) shows that low values of both parameters occur beneath the foreland basin and define a very similar structure. However, the quantitative procedure of *Bedrosian et al.* [2004] was applied to determine if distinct model domains can be identified by ranges of velocity and resistivity.

[24] After interpolation of the resistivity model onto the same grid as the seismic velocity model, and masking poorly resolved areas of both models to avoid correlation of unconstrained parameter estimates, a histogram of the occurrence of resistivity and velocity combinations for each model cell was generated (Figure 4e). Cells within the resistivity model were then determined that contributed to the distinct domains identified within this histogram (Figure 4g).

[25] As observed for central Taiwan (Figures 4f and 4h), three of these domains (CP/WF, HSR and WCR/ECR) identified in the histogram for southern Taiwan (Figures 4e and 4g) reveal a general trend that correlates an increase in resistivity with an increase in the seismic velocity. The link between these parameters is the material porosity; as porosity decreases, both resistivity and velocity increase [*Hacikoylu et al.*, 2006]. This trend is consistent with the eastward increase in metamorphic grade across Taiwan that results in a reduction of porosity. However, the majority of cells that comprise the Lishan Fault Conductor do not plot on this trend. Rather, the LFC domain is characterized by low resistivity (largely equal to values observed in the CP/WF domain) but only moderate seismic velocity. A small percent of interconnected porosity, saturated with saline fluid could explain the low resistivities observed, and would not significantly reduce the P wave velocities [*Jones et al.*, 1998].

[26] Making the same assumptions regarding the fluid composition within the middle crust as for central Taiwan [*Bertrand et al.*, 2009], a saline fluid is expected to have a resistivity within the range $\rho_w \sim 0.01$–0.05 Ωm [*Nesbitt*, 1993]. Using Archie's Law [*Archie*, 1942] with a cementation factor of m = 1.5 requires porosity values of 0.5–1.5% to explain a bulk resistivity of 30 Ωm. Note that a recent sulphide deposit is located between the Chuchih and Lishan Faults, not far north of the southern MT profile [*Lewis et al.*, 2007] (Figure S9). This deposit provides evidence for hydrothermal fluids associated with inferred dehydration reactions within the crust [*Craw et al.*, 2002]. Further, observation and analysis of foliated rocks with extensive veining suggests that the Lishan Fault hosts an active fluid flow system [*Upton et al.*, 2011]. Thus, the LFC in southern Taiwan can be explained by a small percent interconnected porosity saturated with saline fluids, as was the case for the LFC observed in central Taiwan.

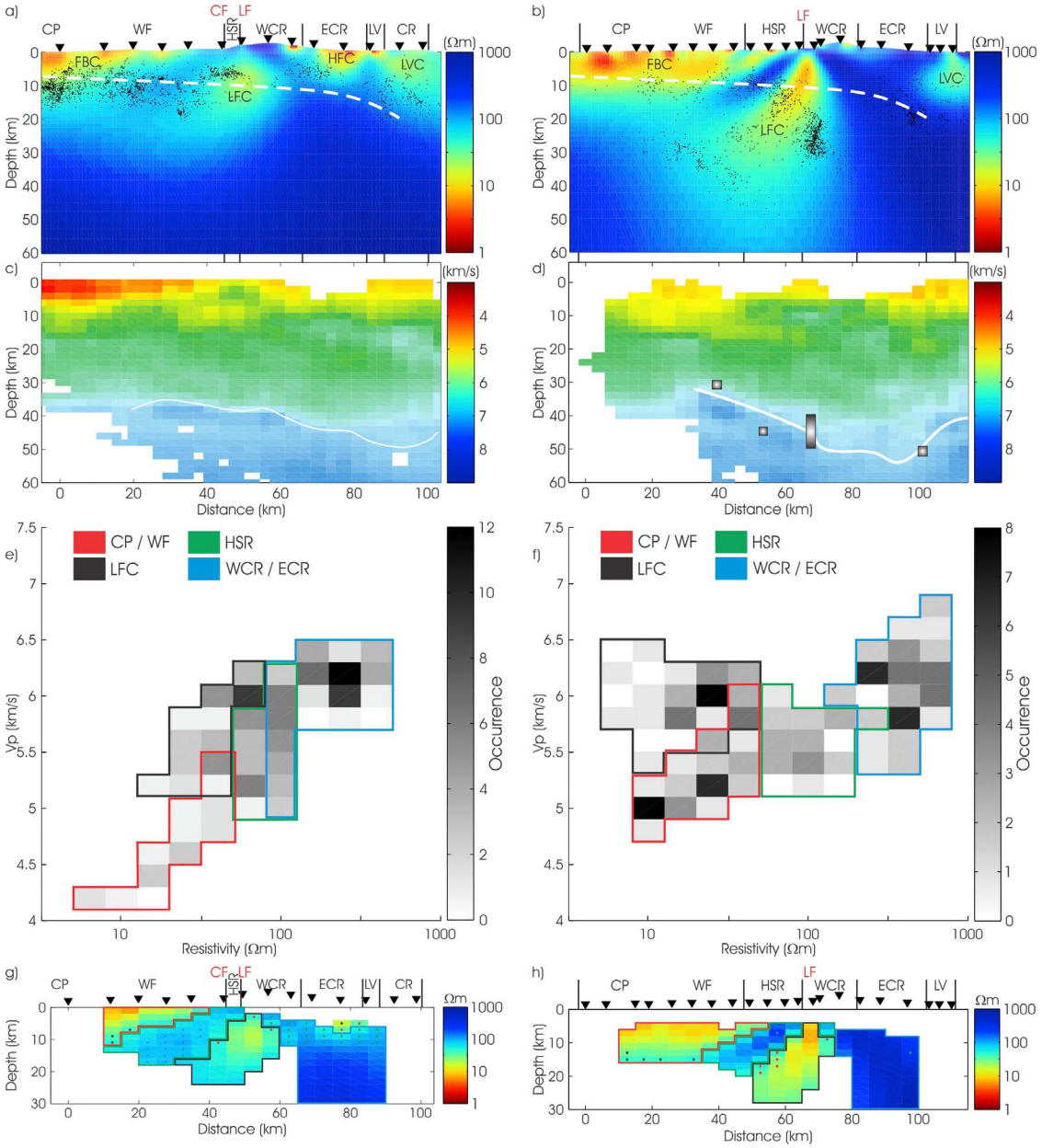

Figure 4. TE, TM, and tipper resistivity inversion model of (a) southern and (b) central Taiwan showing high-quality relocated hypocenters occurring within 20 km of the profiles (data from *Wu et al.* [2008]). Model conductors are abbreviated as follows: FBC, Foreland Basin Conductor; LFC, Lishan Fault Conductor; HFC, Hydrothermal Fluids Conductor; LVC, Longitudinal Valley Conductor. Other abbreviations are defined in Figure 1. Tomographic P wave velocity model for the (c) southern and (d) central Taiwan MT profiles with contour v_p = 7.3 km/s for reference (data from *Wu et al.* [2009]). Vertical gray bars on the central Taiwan model show Moho depth from receiver functions [*Kim et al.*, 2004]. Crossplot of P wave velocity and electrical resistivity for (e) southern and (f) central Taiwan for the above models. Resistivity model of (g) southern and (h) central Taiwan indicating the spatial regions that give rise to the colored domains in the crossplots. Note that white areas indicate where the resistivity and velocity models were masked. Dots indicate cells that contribute to bins within overlapped domains in the histogram.

4.4. Constrained Inversion Results

[27] To support the thick-skinned lithospheric deformation model, it is required to show that the LFC extends to mid-crustal depths in southern Taiwan. However, MT data do not always reliably resolve the depth extent of conductive features, and constrained inversions are required to determine the shallowest conductor consistent with MT data [*Li et al.*, 2003]. Constrained inversions were implemented with the

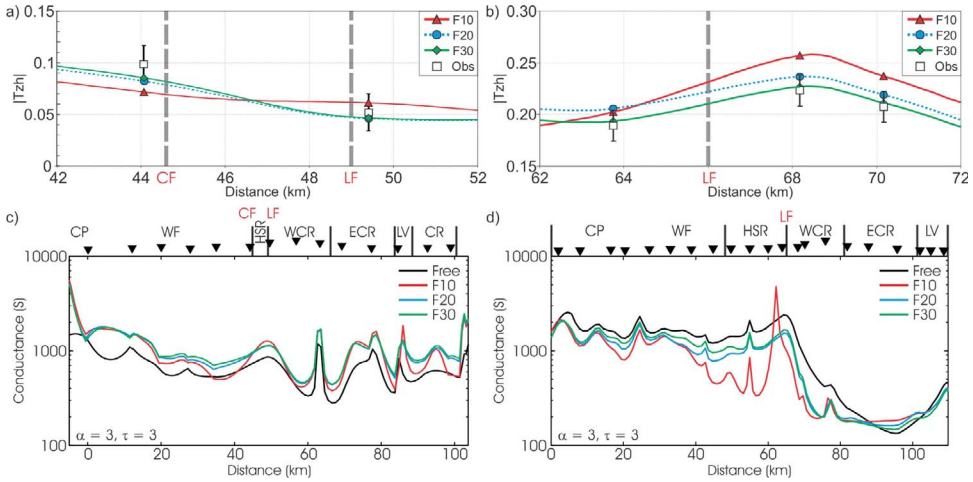

Figure 5. Tipper data parallel to profile at a period of (a) 100 s for southern Taiwan and (b) 30 s for central Taiwan, for stations adjacent the Chuchih Fault CF and Lishan Fault LF. Smooth curves are responses of constrained inversion models with a resistive (300 Ωm) basement fixed at depths 10, 20, and 30 km (models F10, F20, and F30, respectively). Integrated conductance to 60 km depth for the constrained 2-D inversion models of (c) southern and (d) central Taiwan. Smoothing parameters are $\alpha = 3$ and $\tau = 3$.

resistivity models fixed to be resistive (300 Ωm) below depths of 10, 20 and 30 km. The fit to the observed tipper data at a period of 30 s at stations nearest to the Chuchih and Lishan Faults for these constrained inversions are shown in Figure 5a. At a period of 30 s, these tipper data correspond to a depth of ∼15 km, assuming a resistivity of 30 Ωm. Note that since the resistivity of the LFC beneath central Taiwan is lower (∼10 Ωm) the tipper data were analyzed at a period of 100 s (Figure 5b) in order to be sensitive to a comparable depth. Figure 5a shows that both the F30 and F20 models fit the observed data to within the errors. In contrast, the F10 model shows a poor fit to the measured data near the CF and provides evidence that the LFC extends beyond a depth of 10 km in southern Taiwan.

[28] Since MT data are sensitive to conductance, plotting the integrated conductivity along profile can also indicate whether the constrained inversion models are able to fit the measured MT data. Figure 5c reveals that the conductance for the F20 and F30 models are similar, and suggests that these MT data cannot distinguish between a resistive basement at depths of 20 and 30 km. In contrast, the conductance determined for the F10 model is more variable, with the greatest difference occurring beneath the CF and LF. However, the obvious oscillatory behavior observed in the F10 model conductance for central Taiwan (Figure 5d) does not appear in these data. The more subdued difference between the F10 and other constrained inversion models requires a more rigorous approach.

[29] The r.m.s. data misfit quantifies the ability of the constrained inversions to fit the measured MT data. As expected, the misfit progressively decreases as the fixed resistive basement is lowered. However, the reduction in r.m.s. misfit between the F20 and F30 models in southern Taiwan is minimal (0.027). This small reduction is consistent with the observed similarity in these model responses (Figures 5a and 5c) and indicates insensitivity of the southern MT data at these depths. In contrast, a greater reduction in r.m.s. misfit occurs between the F10 and F20 models (0.096), although the magnitude of this reduction is nearly equal to that observed between the F20 and F30 models in central Taiwan (0.098).

[30] Do the MT data in southern Taiwan require that the LFC extend to mid-crustal depths? In central Taiwan, the F10 constrained inversion model was clearly incapable of fitting the measured data. In southern Taiwan, the same analysis suggests that the F10 constrained inversion model does not adequately fit the observed MT data; however, the degree of incompatibility is less than observed in the central MT data.

4.5. Comparison: Southern and Central Taiwan

[31] The Pingtung Plain is located 45 km southwest of the southern MT profile (Figure 1a) and marks the northern limit of the Wadati-Benioff zone associated with subduction at the Manila trench [*Kao et al.*, 2000; *Lacombe et al.*, 2001]. At the northern terminus of this basin, initial contact between the WF and Central Ranges occurs and is thought to reflect the elimination of oceanic lithosphere and initiation of contact between the Eurasian shelf and forearc ridge [*Shyu et al.*, 2005]. Therefore, assuming steady state collision at a propagation rate of 60 km/Myr [*Byrne and Liu*, 2002], the southern MT profile traverses a collision that began ∼0.75 Ma. In contrast, the central MT data cross a more mature orogen resulting from mountain building processes that have occurred for ∼2.5 Myr. Uncertainty in these age estimates exists; *Suppe* [1984] estimated a propagation rate of 90 km/Myr and *Lee et al.* [1991] calculate 40 km/Myr. However, the key point is that the orogen is mature in central Taiwan and developing in the south. Can this difference in the age of collision explain along-strike variations observed in the MT models?

[32] The MT inversion models of southern (Figure 4a) and central Taiwan (Figure 4b) show that similar resistivity structures occur along the strike of the orogen axis. However, at depths of the middle to lower crust, variation between these models occurs in the properties of the Lishan Fault Conductor. Specifically, the LFC extends over a

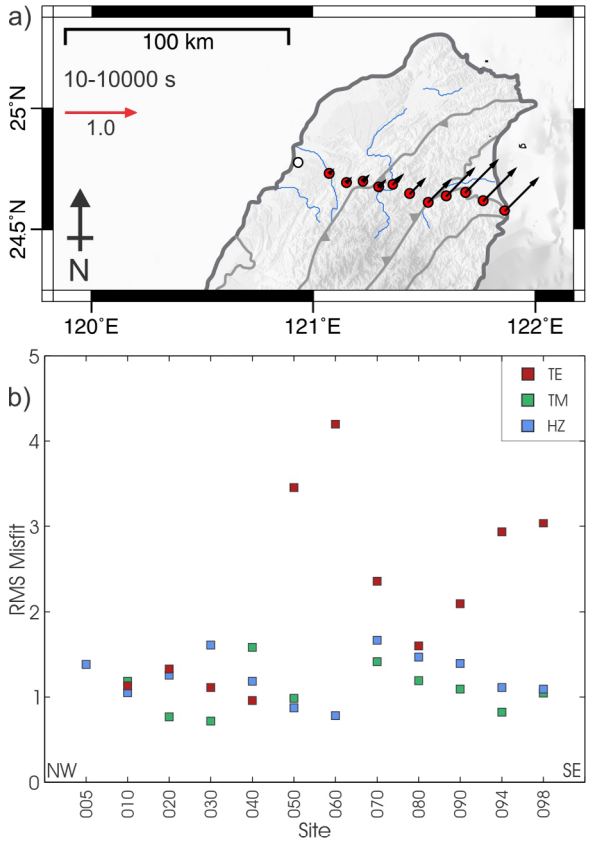

Figure 6. (a) Along-strike (N45°E) components of the real induction vectors plotted in the *Parkinson* [1962] convention and averaged over the period band 10–10000 s. Scale arrow of magnitude 1.0 is shown. (b) R.M.S. data misfit for a 2-D inversion model of northern Taiwan that used the following controls: smoothing parameters $\alpha = 3$ and $\tau = 3$ and error floors of 20%, 7.5%, and 0.03 for the apparent resistivity, phase, and tipper data, respectively. Poor fit is achieved to the TE mode data in northeastern Taiwan, where the greatest along-strike induction vectors were measured.

greater spatial area and shows a lower resistivity in central Taiwan. These observations may be linked to the difference in orogen age between these latitudes. As the processes of deformation and metamorphism occur in the thick-skinned model, it is expected that a greater amount of fluids would exist beneath the more mature orogen in central Taiwan. Approximating the spatial extent of the LFC in central (25 km depth) and southern (15 km depth) Taiwan, and using porosities computed for the range of fluid salinities expected at mid-crustal depths, indicates that roughly twice the quantity of saline fluids is required in central Taiwan (4–8 km^2) in comparison to southern Taiwan (1–4 km^2). These data suggest that the southern MT model yields a snapshot of central Taiwan at ~1.75 Ma.

4.6. Correlation of Resistivity and Hypocenter Locations

[33] Earthquake hypocenters represent an earth response that is sensitive to both material properties and in situ conditions of deformation. Links between resistivity and seismicity have been noted in a number of previous studies, with seismicity commonly occurring at the perimeters of conductors interpreted as zones of fluids [e.g., *Ogawa et al.*, 2001; *Türkoğlu et al.*, 2009; *Wannamaker et al.*, 2009].

[34] Accurately relocated earthquake hypocenters ('A' quality rated events from *Wu et al.* [2008]) within 20 km of the MT profiles are plotted on the resistivity models of southern (Figure 4a) and central Taiwan (Figure 4b). These plots reveal a pattern where the majority of the seismicity is located within the more resistive regions of the MT models. In addition, a cluster of deep (20 - 30 km) seismicity flanks the eastern edge of the LFC in central Taiwan. These events occurred after the Chi-Chi earthquake and focal mechanism solutions suggest that they are associated with a thrust fault, with the Central Ranges on the footwall side [*Wu et al.*, 2004]. *Gourley et al.* [2007] have recognized this and other evidence for deep vertical faults within the Central Ranges that would contribute to building a crustal root in a thick-skinned tectonic regime. The high-angle of these epicenters delineate a steeply dipping fault, far from the angle predicted for failure under dry conditions due to maximum horizontal compressive stress (i.e., 30°) [*Anderson*, 1905]. Thus, the steep dip and the location adjacent the fluid-based LFC suggests that this fault may act as a conduit for fluid migration toward the surface. In southern Taiwan, clusters of events are observed along the western perimeter of the LFC.

[35] Of further interest in Central Taiwan is a zone of deep (30–50 km) events that dip to the east beneath the foreland basin. At these depths, it is likely that these events are occurring within the brittle olivine-rich material below the Moho. The dip toward the hinterland could result from crustal thickening beneath the Central Ranges and also support the thick-skinned tectonic model.

5. A Subducting Collision: Northern Taiwan

[36] North of 23.7°N, contact between the EUP and PSP occurs at progressively greater depth beneath Taiwan. A seismically defined Wadati-Benioff zone places contact between the plates at ~50 km depth at the latitude (~24.7°N) of the northern TAIGER MT profile [*Wu et al.*, 2009]. The 12 northern MT data were subjected to the same rigorous data analysis and inversion procedures that were applied to the southern and central TAIGER MT data (Figures S10 and S11). Of note, the real induction vector components (Figure 6a) indicate that a conductive anomaly occurs beneath the Ilan Plain, the onshore extension of the Okinawa trough (an extending back-arc basin). In addition, a sizable low-velocity anomaly has been observed beneath the Ilan Plain [*Wu et al.*, 2009]. Coincident zones of low resistivity and low velocity have been observed elsewhere in back-arc regions [*Brasse et al.*, 2002; *Hyndman et al.*, 2005; *Soyer and Unsworth*, 2006] and provide evidence for shallow convecting asthenosphere. *Wu et al.* [2009] suggest that the asthenosphere beneath northern Taiwan occurs at a shallow depth (~50 km) and permits the continued westward advance of the PSP due to the oblique plate convergence.

5.1. The 2-D MT Inversion

[37] Initial 2-D inversion models of northern Taiwan showed significantly higher r.m.s. data misfits than for southern and central Taiwan, using the same error floors. Inspection of the data misfits for each mode and station

reveals that the TE mode data in northeastern Taiwan are poorly fit (Figure 6b), where the induction vectors point to 3-D resistivity structure. Since the TE mode data are most susceptible to off-profile effects, in 3-D regions it is common to down-weight TE mode data by increasing their error floors in comparison to the TM mode values [*Heise et al.*, 2007]. Thus, the TE mode data in Northern Taiwan were downweighted by increasing their error floors to 40% for the apparent resistivity and 4.4° for the phase. A final 2-D inversion model of the northern MT impedance and tipper data produced an r.m.s. data misfit of 1.152 (Figure 7a).

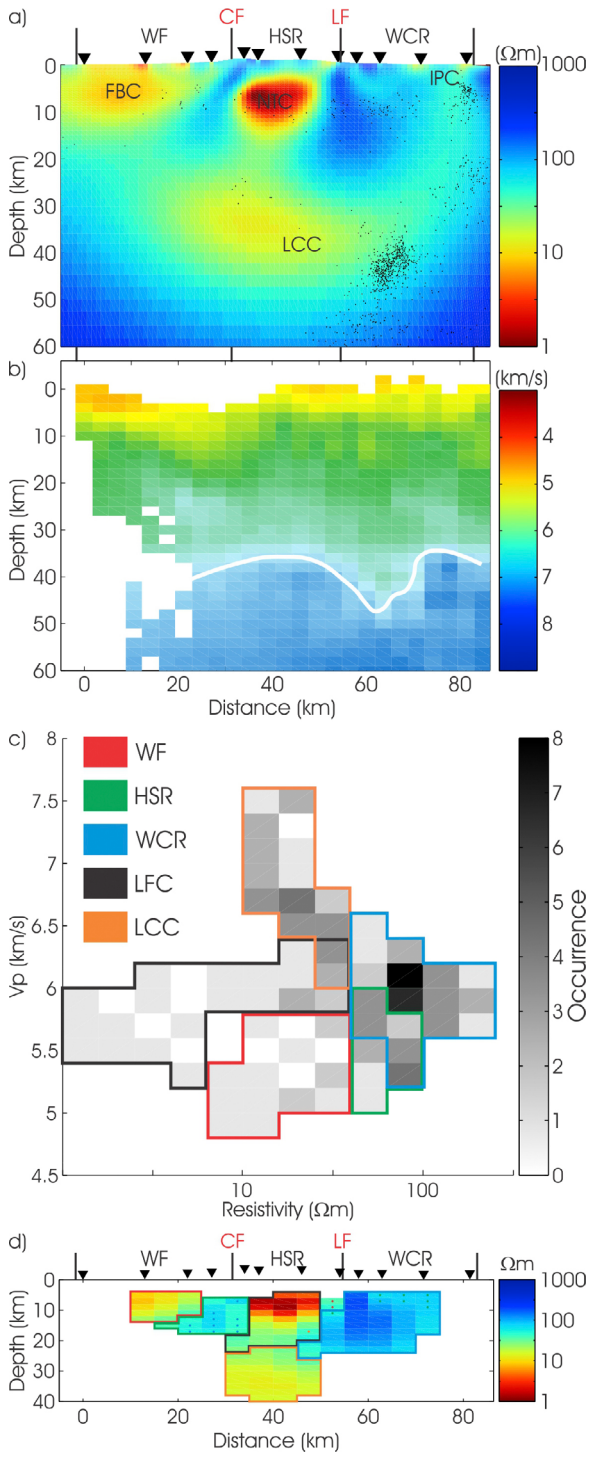

Figure 7. (a) TE, TM, and tipper resistivity inversion model of northern Taiwan showing high-quality relocated hypocenters occurring within 20 km of the profile (data from *Wu et al.* [2008]). Model conductors are abbreviated as follows: FBC, Foreland Basin Conductor; NTC, Northern Taiwan Conductor; LCC, Lower Crustal Conductor; IPC, Ilan Plain Conductor. Other abbreviations are defined in Figure 1. (b) Tomographic P wave velocity model for the northern Taiwan MT profiles with contour v_p = 7.3 km/s for reference (data from *Wu et al.* [2009]). (c) Crossplot of P wave velocity and electrical resistivity for the models in Figures 7a and 7b. (d) Resistivity model of Figure 7a indicating the spatial regions that give rise to the colored domains in the crossplots. Note that white areas indicate where the resistivity and velocity model were masked. Dots indicate cells that contribute to bins within overlapped domains in the histogram.

5.2. Resistivity Model Interpretation

[38] In northwestern Taiwan, low resistivities occur within the upper 10 km beneath the Western Foothills province (FBC in Figure 7a), and can be explained by fluid filled porosity within the sedimentary rocks of the foreland basin. East of this zone, the Chuchih Fault marks uplift of the high mountain ranges that expose metamorphic rocks of increasing grade toward the east. A reduction in porosity associated with these crystalline metamorphic materials correlates with the general eastward increase in resistivity observed in the near-surface.

[39] Near the east coast, low resistivity occurs (IPC in Figure 7a) that coincides with a low velocity anomaly reported beneath the Ilan Plain [*Wu et al.*, 2009]. Located above the Wadati-Benioff zone, it is likely that the low resistivity in this zone is due to fluids released from the subducting slab. At this latitude, the subducting PSP is located at a depth of ~50 km [*Wu et al.*, 2009], and within the stability field for dewatering reactions in greenschist and lower amphibolite facies [*Wannamaker et al.*, 2009]. However, located at the edge of the profile, and where the measured MT data showed significant 3-D effects, constraints on this diffuse zone of low resistivity are poor. Below the Hseuhshan range, a strong upper crustal conductor is imaged (NTC – Northern Taiwan Conductor, in Figure 7a) that laterally terminates below the surface expressions of the Chuchih and Lishan Faults. The properties of the NTC are best explained by interconnected saline fluids. Note that despite some uncertainty in the surface heat flow estimates, *Song and Ma* [2002] determined a preferred geothermal gradient for the Central Ranges of ~17°C/km. This gradient places the solidus (650°C) of wet felsic rocks [*Vanyan and Gliko*, 1999] at a depth of 38 km, eliminating partial melt as an explanation for this low-resistivity feature.

[40] Comparison of the geometry and location of the LFC in southern and central Taiwan with the NTC in northern Taiwan reveals along-strike variations. Namely, the LFC was centered below the Lishan Fault in southern and central Taiwan, while the NTC occurs west of this fault below the northern profile. In addition, while the conductance of the NTC continues the observed trend of increasing conductance associated with the age of collision, a simple extension of the

LFC may not be appropriate for northern Taiwan where plate collision occurs at depth. It may be more reasonable to associate the NTC with fluids in a back-arc region sourced from dewatering of the subducting Philippine slab. For these reasons, the upper crustal conductor beneath northern Taiwan is distinguished as the NTC.

[41] Finally, a broad zone of low resistivity is imaged that dips moderately eastward at lower crustal depths (LCC – Lower Crustal Conductor, in Figure 7a). Resolution of this feature is poor owing to its location below the shallower prominent NTC. For MT data to resolve a deeper conductor overlain by a shallow conductor, the conductance of the lower conductor must be greater than that of the upper one. Clearly, the conductance of the NTC (10 km / 3 Ωm ∼ 3333 S) is greater than the LCC (15 km / 10 Ωm ∼ 1500 S), and the resulting poor sensitivity at depth can explain the lower crustal variability in the inversion models shown in Figure S10. While characteristics of the LCC are poorly constrained, all inversion models show a broad zone of low resistivity at ∼30 km depth that dips to the east (Figure S10). In addition, constrained inversion tests (Figure S12) show that low-resistivity is required at 30–40 km depths, and that the LCC is likely a robust feature of the model.

5.3. Correlation of Resistivity and Seismic Velocity

[42] Ore bodies cannot account for large spatial zones of high conductivity as observed beneath northern Taiwan (NTC and LCC in Figure 7a). Further, graphite is unlikely to maintain a connected network within an active orogen [*Katsube and Mareschal*, 1993; *Wannamaker*, 2000]. Therefore, two possible sources are left to explain these observed conductors: interconnected saline fluids or partial melt.

[43] Temperature is often the key parameter required to discriminate between aqueous fluids and partial melt [*Brasse et al.*, 2002]. Unfortunately, heat flow data in Taiwan are sparse in the high mountain ranges, and contaminated by the effects of groundwater circulation [*Song and Ma*, 2002]. Therefore, to increase constraints on model features, the northern MT resistivity model (Figure 7a) was plotted with a coincident tomographic model of P wave velocity (Figure 7b) that consists of $5 \times 5 \times 2$ km^3 blocks (in x, y and z directions) and includes first arrival data from the TAIGER active seismic transects collected in 2007–8. These independently derived models were quantitatively correlated with the procedure of *Bedrosian et al.* [2004], and reveal a consistent trend of increasing resistivity and velocity eastward across the island (identified by the WF, HSR and WCR domains in Figures 7c and 7d). Since the grade of metamorphism increases eastward across Taiwan, an associated reduction in porosity can explain this observed trend [*Hacikoylu et al.*, 2006]. However, model cells that comprise the NTC plot off this trend in a distinct zone identified by low resistivity and moderate seismic velocity. Note that the velocity ranges (5.25–6.5 km/s) that define the LFC domains in southern (Figure 4e) and central Taiwan (Figure 4f) are consistent with the NTC domain in northern Taiwan (Figure 7c). Using Archie's Law [*Archie*, 1942], porosities of 2–6% are required to explain the resistivity (3 Ωm) of the NTC in northern Taiwan, assuming pore fluid salinities within the range ρ_w = 0.01–0.05 Ωm [*Nesbitt*, 1993] and a cementation exponent of m = 1.5. The source of the NTC in northern Taiwan is therefore consistent with a small percent interconnected porosity saturated with saline fluids.

[44] Detailed explanation of the Lower Crustal Conductor is difficult due to a lack of high resolution data required to constrain properties of the lower crust beneath northern Taiwan. For example, the change in velocity across the Moho beneath Taiwan is not yet reliably determined, although contours of v_p = 7.5 km/s in tomographic models have been used as a guide [*Wu et al.*, 2009]. Therefore, since the LCC domain is characterized by P wave velocities that are below 7.5 km/s, this supports the location of this feature within a thickened lower crust. Using the proposed average geothermal gradient (∼17°C/km) [*Song and Ma*, 2002] permits partial melting of wet felsic material at a depth of ∼38 km. This estimate defines a lower limit; modeling fission track ages indicates a geothermal gradient of 20–25°C/km [*Willett et al.*, 2003]. These geothermal gradients place the solidus of wet felsic material (650°C) [*Vanyan and Gliko*, 1999] within the depths of 30–40 km where the LCC is constrained to occur. These data reveal that aqueous fluids are required to explain the low resistivity observed in the LCC. In contrast, partial melt can contribute but is not required. Note that temperatures greater than 1000°C are required to melt dry crustal materials [*Vanyan and Gliko*, 1999], and the absence of aqueous fluids would eliminate the possibility of melting at depths of 30–40 km.

5.4. Correlation of Resistivity and Hypocenter Locations

[45] Do the same mechanisms of prograde metamorphism within a thickening crust that provide the source of crustal aqueous fluids in southern and central Taiwan also operate in the north? Contact between the converging Philippine Sea and Eurasian Plates occurs from the surface down in southern and central Taiwan. In contrast, at the latitude of the northern MT profile, contact occurs at a depth of ∼50 km [*Wu et al.*, 2009]. Therefore, whole lithosphere-scale convergence does not occur in northern Taiwan. However, subduction of the fluid-rich oceanic crust provides a source of fluids at depth that is not present further south.

[46] Plotting high-quality relocated hypocenters [*Wu et al.*, 2008] that locate within 20 km of the northern MT profile reveals a strong correlation between model conductors and aseismic zones (Figure 7a). In addition, a cluster of events occurs along the eastern margin of the LCC at depths of 40–50 km that marks convergence of the subducting PSP [*Wu et al.*, 2009]. Occurring at the edge of this conductor suggests that these events may promote the release of fluids from the downgoing slab. The eastward dip of the LCC suggests that the Philippine slab is an important source of fluids beneath northern Taiwan.

6. Discussion

6.1. The Lishan Fault Conductor

[47] The debate over which end-member tectonic model is applicable in central Taiwan was advanced by analysis of the LFC imaged with TAIGER MT data. *Bertrand et al.* [2009] showed that this feature was inconsistent with the thin-skinned model, since thin-skinned deformation is inconsistent with a wide zone of distributed interconnected saline

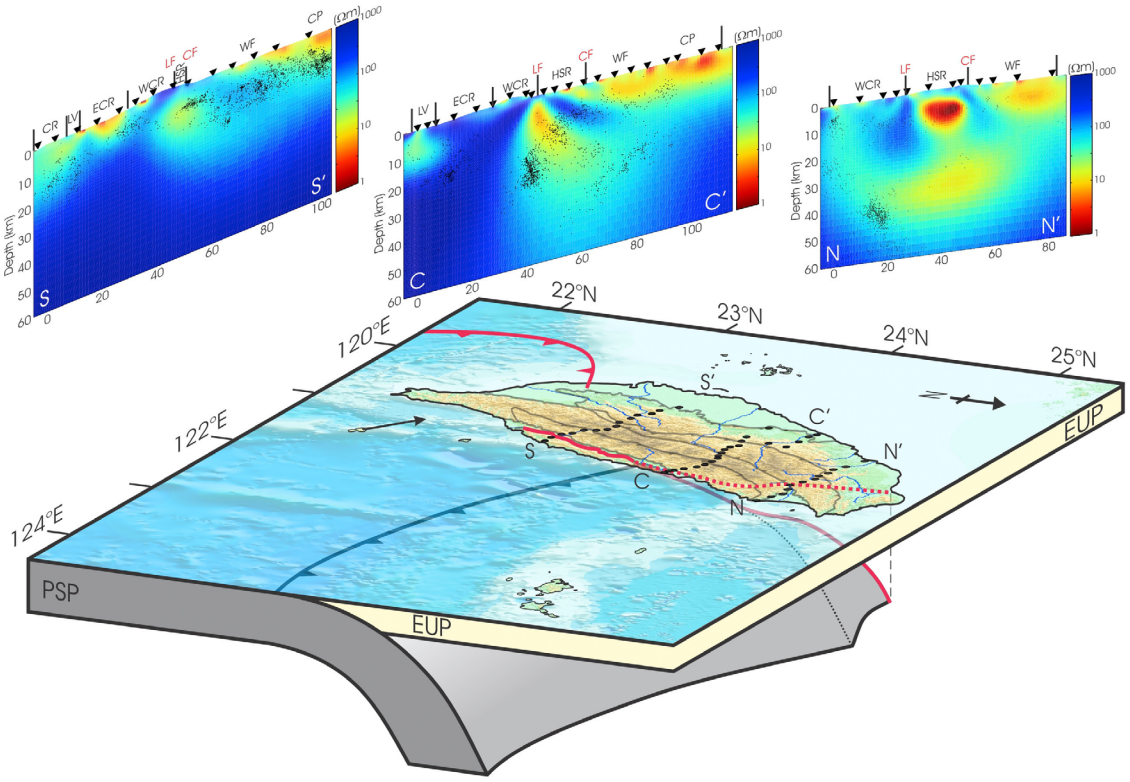

Figure 8. A 3-D schematic of plate convergence in the Taiwan region. The solid red line defines the western boundary of the Philippine Sea Plate. The final 2-D resistivity models from the TAIGER MT data analyzed (black dots) are shown at the top for comparison. Seismicity data are from *Wu et al.* [2008]; only events with the highest quality relocation grade (A) are shown. Beneath northern Taiwan, the Eurasian plate is absent and likely removed by slab break-off.

fluids that crosses the inferred décollement at 10 km depth [*Carena et al.*, 2002]. In contrast, the thick-skinned tectonic model predicts deformation to occur on lithospheric scales resulting in dehydrating prograde metamorphic reactions as the crust is thickened [*Wannamaker et al.*, 2002]. These reactions could provide the source of fluids in the middle and lower crust required to explain the LFC.

[48] *Anderson*'s [1905] theory of faulting predicts that thrust faults should form with a dip angle of 30° for maximum horizontal compressive stress. However, this theory is not universally applicable; if conditions are favorable, a pre-existing fault may be reactivated rather than initiation of a new fault. In Taiwan, Cenozoic rifting has left a legacy of normal faults in the passive margin of Eurasia that are now largely obscured by Pliocene-Pleistocene sediment from the adjacent orogen [*Lee et al.*, 2002]. For example, the Lishan Fault is interpreted as an inverted passive margin growth fault that shows oblique thrust movement [*Angelier et al.*, 1990; *Clark et al.*, 1993; *Lee et al.*, 1997]. Inversion of rift-related high-angle faults highlights the importance of pre-existing features in the development of the Taiwan orogen. In general, inversion can result in thick-skinned tectonics. Steeply dipping clusters of seismicity beneath the Central Ranges that show thrust fault focal mechanisms provide further evidence for deep collision-related deformation [*Lee et al.*, 2002; *Gourley et al.*, 2007].

[49] Note that an additional MT profile located between the southern and central TAIGER transects would be useful to map the along-strike continuity of the LFC. However, the similarity between the resistivity models in southern and central Taiwan supports the thick-skinned lithospheric deformation model for the orogen between ~23–24°N latitude. Further, the lesser conductance of the LFC in the south correlates with the time-axis of orogen evolution that follows the island strike. Uniformitarianism [*Lyell*, 1830] provides the simple explanation that the southern MT model represents a glimpse of central Taiwan at ~1.75 Ma. The ongoing deformation and dehydrating metamorphism within a developing crustal root have occurred longer in central Taiwan, and result in the greater present-day conductance observed in the middle and lower crust. These results are supported by tomographic seismic velocity models which indicate that the crustal root beneath central Taiwan shallows to the south [*Rau and Wu*, 1995].

6.2. The Subducting Indenter: Dewatering of the Philippine Slab

[50] Beneath northern Taiwan at the latitude of the TAIGER MT profile (~24.7°N), the obliquely subducting PSP contacts the EUP at a depth of ~50 km [*Wu et al.*, 2009]. At this location, deformation due to the converging plates significantly differs in comparison to locations south of 23.7°N, where contact occurs from the surface down. The subducting indenter causes compression west of the plate contact, but permits extension to develop in the overlying Eurasian wedge, clearly expressed at the surface by the Ilan Plain. The

resistivity model of northern Taiwan shows significant variations in comparison to the models of southern and central Taiwan that can be explained by the subducting indenter tectonic model (Figure 8).

6.2.1. The Lower Crustal Conductor

[51] A distributed zone of conductivity with down-to-the-east dip is imaged in the lower crust beneath northern Taiwan at ~30–50 km depth. The diffuse eastern boundary of this zone coincides with a cluster of seismicity that marks the subducting PSP slab. While the uncertain temperature regime may permit partial melt to contribute to the low resistivities in this zone, saline aqueous fluids are required. The pattern of seismicity occurring at the perimeter of this conductor suggests that these events promote dewatering of the slab and fluid mobilization toward the surface. At depths of 40–60 km, greenschist and lower amphibolite facies within a subducting slab undergo dehydration metamorphic reactions [*Wannamaker et al.*, 2009]. However, a thickened crust beneath northern Taiwan (40–50 km) [*Wu et al.*, 2009] suggests that remnant fluids released by prograde metamorphic reactions could also be present. Offshore northwestern Taiwan, sediments in the Taishi-Taichung basin [*Lin et al.*, 2003] represent a source of fluids that could be released by metamorphism during subduction and deformation of the Eurasian margin. Two sources of fluids are therefore possible in northern Taiwan to account for the low-resistivity structures observed.

6.2.2. The Northern Taiwan Conductor

[52] Is the NTC the along-strike continuation of the LFC identified in southern and central Taiwan? Furthermore, the LFC was attributed to fluids released by prograde metamorphism within a thickening crust due to deformation caused by plate convergence. Do these same processes explain the NTC? Unfortunately, additional MT data between the northern and central TAIGER profiles are required to unequivocally resolve these questions. However, the NTC is located ~60 km south of the Tatun Volcanic Group (Figure 1a), which recorded episodic volcanism during 2.8–0.2 Ma [*Kim et al.*, 2005] within the extensional back-arc region of the Ryukyu subduction zone. Given that the Tatun volcanoes have been dormant for 0.2 Myr and that the Ryukyu trench is propagating southwards, the NTC may be related more to extension within the back-arc region of the Ryukyu subduction zone, rather than crustal deformation processes below. That this zone of high conductivity is explained by fluids suggests significant weakening of the crust may be occurring – perhaps foreshadowing the location of future Ryukyu back-arc volcanism.

6.3. Crustal Fluids

[53] Small quantities of saline fluids (~0.5–2% saturated porosity) have been proposed to explain the presence of major crustal conductive features imaged beneath Taiwan. However, to lower the resistivity below a few 100 Ωm requires that these fluids are interconnected through fracture networks, and/or grain edge wetting [*Jiracek et al.*, 2007]. Within ductile shear zones, saline fluids are likely to interconnect through grain-edge wetting [*Holness*, 1993; *Tullis et al.*, 1996] since salts significantly lower the dihedral angle to ~40° [*Watson and Brenan*, 1987], which is below that required for interconnection (60°) in low porosity (<1%) rocks [*Watson et al.*, 1990]. In addition, extensional fracture networks can initiate perpendicular to the minimum principal stress direction for elevated fluid pressures [*Cox*, 2005]. Thus, in compressional tectonic environments, extensional cracks form horizontally and can cause widespread zones of low resistivity. Clearly, to explain the broad regions of crustal conductivity beneath Taiwan requires pervasive shear to promote fluid interconnection, and supports the lithospheric-scale deformation model.

7. Conclusions

[54] The TAIGER MT data have provided information that was used to constrain the style of tectonics operating beneath southern [*Chiang et al.*, 2010] and central [*Bertrand et al.*, 2009] Taiwan. In addition, comparison of the MT profiles collected in southern and central Taiwan provide a guide to the evolution of the arc-continent collision and indicate that the young orogen is developing through the same manner of thick-skinned lithospheric deformation. Finally, the TAIGER MT data collected in northern Taiwan indicate along-strike variations in the electrical resistivity structures that have been linked with the subducting indentation of the Philippine Sea Plate on the Eurasian Plate at progressively greater depths to the north.

[55] Throughout Taiwan, saline fluids have been shown to explain key crustal low resistivity features. Fluids, even in small quantities, strongly lower both the electrical resistivity and the strength of lithospheric materials. Therefore, the MT technique is a particularly useful tool in active tectonic environments to map the location of fluids, and by extension, zones of weakness where deformation is localized.

[56] In Taiwan, the crustal conductance observed beneath the TAIGER MT profiles increases progressively toward the north. The greatest conductance recorded beneath northern Taiwan indicates a widespread concentration of fluids within the lower crust sourced from deformation during crustal thickening and from dewatering of the subducting PSP slab. This widespread zone of fluids could facilitate the reorganization of this plate boundary. Extension in northern Taiwan, due to slab suction and rollback of the Ryukyu trench, is propagating on land and chasing the convergence to the south. Beneath central and southern Taiwan, fluids map a pervasive zone of collisional deformation that is lithospheric in scale.

[57] **Acknowledgments.** This research was funded by the National Sciences and Engineering Research Council of Canada, National Science Foundation (Continental Dynamics Program) under award EAR0410227 and EAR1010645, Alberta Ingenuity Fund, National Central University of Taiwan and the University of Alberta, Canada. Assistance from land owners in Taiwan is appreciated. We thank Randy Mackie for use of his 2-D inversion algorithm, Weerachai Siripunvaraporn for use of his 3-D inversion program, and Alan Jones and Gary McNeice for their tensor decomposition software.

References

Anderson, E. M. (1905), *The Dynamics of Faulting*, Oliver and Boyd, London.

Angelier, J., F. Bergerat, H. T. Chu, and T. Q. Lee (1990), Tectonic analysis and the evolution of a curved collision belt: The Hsüehshan range, northern Taiwan, *Tectonophysics*, *183*, 77–96, doi:10.1016/0040-1951(90)90189-F.

Archie, G. E. (1942), The electrical resistivity log as an aid in determining some reservoir characteristics, *Trans. Am. Inst. Min. Metall. Eng.*, *146*, 54–62.

Barrier, E., and J. Angelier (1986), Active collision in eastern Taiwan: The Coastal range, *Tectonophysics*, *125*, 39–72, doi:10.1016/0040-1951(86)90006-5.

Bedrosian, P. A., M. J. Unsworth, G. D. Egbert, and C. H. Thurber (2004), Geophysical images of the creeping segment of the San Andreas Fault: Implications for the role of crustal fluids in the earthquake process, *Tectonophysics*, *385*, 137–158, doi:10.1016/j.tecto.2004.02.010.

Bertrand, E. A., M. J. Unsworth, C. W. Chiang, C. S. Chen, C. C. Chen, F. T. Wu, E. Türkoğlu, H. L. Hsu, and G. J. Hill (2009), Magnetotelluric evidence for thick-skinned tectonics in central Taiwan, *Geology*, *37*, 711–714, doi:10.1130/G25755A.1.

Bos, A. G., W. Spakman, and M. C. J. Nyst (2003), Surface deformation and tectonic setting of Taiwan inferred from a GPS velocity field, *J. Geophys. Res.*, *108*(B10), 2458, doi:10.1029/2002JB002336.

Brasse, H., P. Lazeta, V. Rath, K. Schwalenberg, W. Soyer, and V. Haak (2002), The Bolivian Altiplano conductivity anomaly, *J. Geophys. Res.*, *107*(B5), 2096, doi:10.1029/2001JB000391.

Byrne, T. B., and C. S. Liu (2002), Introduction to the geology and geophysics of Taiwan, in *Geology and Geophysics of an Arc-Continent Collision, Taiwan*, edited by T. B. Byrne and C. S. Liu, *Spec. Pap. Geol. Soc. Am.*, *358*, v–viii.

Carena, S., J. Suppe, and H. Kao (2002), Active detachment of Taiwan illuminated by small earthquakes and its control of first-order topography, *Geology*, *30*, 935–938, doi:10.1130/0091-7613(2002)030<0935:ADOTIB>2.0.CO;2.

Chai, B. H. T. (1972), Structure and tectonic evolution of Taiwan, *Am. J. Sci.*, *272*, 389–422, doi:10.2475/ajs.272.5.389.

Chapple, W. M. (1978), Mechanics of thin-skinned fold-and-thrust belts, *Geol. Soc. Am. Bull.*, *89*, 1189–1198, doi:10.1130/0016-7606(1978)89<1189:MOTFB>2.0.CO;2.

Chiang, C. W., C. C. Chen, M. J. Unsworth, E. A. Bertrand, C. S. Chen, T. D. Kieu, and H. L. Hsu (2010), The deep electrical structure of southern Taiwan and its tectonic implications, *Terr. Atmos. Oceanic Sci.*, *21*, 879–895, doi:10.3319/TAO.2010.02.25.01(T).

Chou, Y. W., and H. S. Yu (2002), Structural expressions of flexural extension in the arc-continent collisional foredeep of western Taiwan, in *Geology and Geophysics of an Arc-Continent Collision, Taiwan*, edited by T. B. Byrne and C. S. Liu, *Spec. Pap. Geol. Soc. Am.*, *358,* 1–12.

Clark, M. B., D. M. Fisher, C. Y. Lu, and C. H. Chen (1993), Kinematic analysis of the Hseuhshan range, Taiwan: A large scale pop-up structure, *Tectonics*, *12*, 205–207, doi:10.1029/92TC01711.

Cox, S. F. (2005), Coupling between deformation, fluid pressures, and fluid flow in ore-producing hydrothermal systems at depth in the crust, in *Economic Geology 100th Anniversary Volume*, edited by J. W. Hedenquist et al., pp. 39–76, Soc. of Econ. Geol., Littleton, Colo.

Craw, D., P. O. Koons, T. Horton, and C. P. Chamberlain (2002), Tectonically driven fluid flow and gold mineralization in active collisional orogenic belts: Comparison between New Zealand and western Himalaya, *Tectonophysics*, *348*, 135–153, doi:10.1016/S0040-1951(01)00253-0.

Ernst, W. G., C. S. Ho, and J. G. Liou (1985), Rifting, drifting, and crustal accretion in the Taiwan sector of the Asiatic continental margin, in *Tectonostratigraphic Terranes of the Circum-Pacific Region*, edited by D. G. Howell, pp. 375–389, Am. Assoc. of Pet. Geol., Wayne, Pa.

Fisher, D. M., C. Y. Lu, and H. T. Chu (2002), Taiwan slate belt: Insights into the ductile interior of an arc-continent collision, in *Geology and Geophysics of an Arc-Continent Collision, Taiwan*, edited by T. B. Byrne and C. S. Liu, *Spec. Pap. Geol. Soc. Am.*, *358*, 93–106.

Fisher, D. M., S. Willet, E. C. Yeh, and M. Brooks Clark (2007), Cleavage fronts and fans as reflections of orogen stress and kinematics in Taiwan, *Geology*, *35*, 65–68, doi:10.1130/G22850A.1.

Fuller, C. W., S. D. Willett, and D. M. Fisher (2002), Exhumational steady state in Taiwan: Quantification through thermomechanical modeling, *Eos Trans. AGU*, *83*(47), Fall Meet. Suppl., Abstract T71A-1151.

Gamble, T. D., W. M. Goubeau, and J. Clarke (1979), Magnetotellurics with a remote reference, *Geophysics*, *44*, 53–68, doi:10.1190/1.1440923.

Gourley, J. R., T. Byrne, Y. C. Chan, F. Wu, and R. J. Rau (2007), Fault geometries illuminated from seismicity in central Taiwan: Implications for crustal scale structural boundaries in the northern central range, *Tectonophysics*, *445*, 168–185, doi:10.1016/j.tecto.2007.08.013.

Hacikoylu, P., J. Dvorkin, and G. Mavko (2006), Resistivity-velocity transforms revisited, *Leading Edge*, *25*, 1006–1009, doi:10.1190/1.2335159.

Heise, W., H. M. Bibby, T. G. Caldwell, S. C. Bannister, Y. Ogawa, S. Takakura, and T. Uchida (2007), Melt distribution beneath a young continental rift: The Taupo volcanic zone, New Zealand, *Geophys. Res. Lett.*, *34*, L14313, doi:10.1029/2007GL029629.

Hickman, J. B., D. V. Wiltschko, J. H. Hung, P. Fang, and Y. Bock (2002), Structure and evolution of the active fold-and-thrust belt of southwestern Taiwan from global positioning system analysis, in *Geology and Geophysics of an Arc-Continent Collision, Taiwan*, edited by T. B. Byrne and C. S. Liu, *Spec. Pap. Geol. Soc. Am.*, *358*, 75–92.

Holness, M. B. (1993), Temperature and pressure dependence of quartz-aqueous fluid dihedral angles: The control of adsorbed H_2O on the permeability of quartzites, *Earth Planet. Sci. Lett.*, *117*, 363–377, doi:10.1016/0012-821X(93)90090-V.

Huang, C. Y., P. B. Yuan, C. W. Lin, T. K. Wang, and C. P. Chang (2000), Geodynamic processes of Taiwan arc-continent collision and comparison with analogs in Timor, Papua New Guinea, Urals and Corsica, *Tectonophysics*, *325*, 1–21, doi:10.1016/S0040-1951(00)00128-1.

Hyndman, R. D., C. A. Currie, and S. P. Mazzotti (2005), Subduction zone backarcs, mobile belts, and orogenic heat, *GSA Today*, *15*, 4–10.

Ichihara, H., and T. Mogi (2009), A realistic 3-D resistivity model explaining anomalous large magnetotelluric phases: The L-shaped conductor model, *Geophys. J. Int.*, *179*, 14–17, doi:10.1111/j.1365-246X.2009.04310.x.

Jiracek, G. R., V. M. Gonzalez, T. G. Caldwell, P. E. Wannamaker, and D. Kilb (2007), Seismogenic, electrically conductive, and fluid zones at continental plate boundaries, in New Zealand, Himalaya, and California-USA, in *A Continental Plate Boundary: Tectonics of South Island, New Zealand*, *Geophys. Monogr. Ser.*, vol. 175, edited by D. Okaya, T. Stern, and F. Davey, pp. 347–369, AGU, Washington, D. C.

Jones, S. M., C. McCann, T. R. Astin, and J. Sothcott (1998), The effects of pore-fluid salinity on ultrasonic wave propagation in sandstones, *Geophysics*, *63*, 928–934, doi:10.1190/1.1444404.

Kao, H., G. C. Huang, and C. S. Liu (2000), Transition from oblique subduction to collision in the northern Luzon arc-Taiwan region: Constraints from bathymetry and seismic observations, *J. Geophys. Res.*, *105*, 3059–3079, doi:10.1029/1999JB900357.

Karato, S. I., and H. R. Wenk (2002), *Plastic Deformation of Minerals and Rocks*, *Rev. Mineral. Geochem.*, vol. 51, Mineral. Soc. of Am., Washington, D. C.

Katsube, T. J., and M. Mareschal (1993), Petrophysical modeling of deep electrical conductors: Graphite lining as a source and its disconnection due to uplift, *J. Geophys. Res.*, *98*, 8019–8030, doi:10.1029/92JB02864.

Kim, K. H., J. M. Chiu, H. Konn, Q. Liu, and Y. H. Yeh (2004), A preliminary study of crustal structure in Taiwan region using receiver function analysis, *Geophys. J. Int.*, *159*, 146–164, doi:10.1111/j.1365-246X.2004.02344.x.

Kim, K. H., C. H. Chang, K. F. Ma, J. M. Chiu, and K. C. Chen (2005), Modern seismic observations in the Tatun volcano region of northern Taiwan: Seismic/volcanic hazard adjacent to the Taipei metropolitan area, *Terr. Atmos. Oceanic Sci.*, *16*, 579–594.

Lacombe, O., F. Mouthereau, J. Angelier, and B. Deffontaines (2001), Structural, geodetic and seismological evidence for tectonic escape in SW Taiwan, *Tectonophysics*, *333*, 323–345, doi:10.1016/S0040-1951(00)00281-X.

Ledo, J. (2005), 2-D versus 3-D magnetotelluric data interpretation, *Surv. Geophys.*, *26*, 511–543, doi:10.1007/s10712-005-1757-8.

Lee, C. I., Y. L. Chang, and M. P. Coward (2002), Inversion tectonics of the fold-and-thrust belt western Taiwan, in *Geology and Geophysics of an Arc-Continent Collision, Taiwan*, edited by T. B. Byrne and C. S. Liu, *Spec. Pap. Geol. Soc. Am.*, *358*, 13–30.

Lee, J. C., J. Angelier, and H. T. Chu (1997), Polyphase history and kinematics of a complex major fault zone in the northern Taiwan mountain belt: The Lishan fault, *Tectonophysics*, *274*, 97–115, doi:10.1016/S0040-1951(96)00300-9.

Lee, T. Q., C. Kissel, E. Barrier, C. Laj, and W. R. Chi (1991), Paleomagnetic evidence for a diachronous clockwise rotation of the Coastal Range, eastern Taiwan, *Earth Planet. Sci. Lett.*, *105*, 245–257.

Lewis, C., D. Ray, and K. K. Chiu (2007), Primary geologic sources of arsenic in the Chianan Plain (Blackfoot Disease area) and the Lanyang Plain of Taiwan, *Int. Geol. Rev.*, *49*, 947–961, doi:10.2747/0020-6814.49.10.947.

Li, S., M. J. Unsworth, J. R. Booker, W. Wei, H. Tan, and A. G. Jones (2003), Partial melt and or aqueous fluid in the mid-crust of southern Tibet? Constraints from INDEPTH magnetotelluric data, *Geophys. J. Int.*, *153*, 289–304, doi:10.1046/j.1365-246X.2003.01850.x.

Lin, A. T., A. B. Watts, and S. P. Hasselbow (2003), Cenozoic stratigraphy and subsidence history of the South China Sea margin in the Taiwan region, *Basin Res.*, *15*, 453–478, doi:10.1046/j.1365-2117.2003.00215.x.

Lyell, C. (1830), *Principles of Geology, Being an Attempt to Explain the Former Changes of the Earth's Surface, by Reference to Causes Now in Operation*, vol. 1, 22, John Murray, London.

Malavieille, J., S. E. Lallemand, A. D. Dominguez, C. Y. Lu, C. S. Liu, P. Schnurle and the ACT Scientific Crew (2002), Arc-continent collision in Taiwan: New marine observations and tectonic evolution, in *Geology and Geophysics of an Arc-Continent Collision, Taiwan*, edited by T. B. Byrne and C. S. Liu, *Spec. Pap. Geol. Soc. Am.*, *358*, 187–211.

McIntosh, K., Y. Nakamura, T. K. Wang, R. C. Shih, A. Chen, and C. S. Liu (2005), Crustal-scale seismic profiles across Taiwan and the western

Philippine Sea, *Tectonophysics*, *401*, 23–54, doi:10.1016/j.tecto.2005.02.015.

Mouthereau, F., B. Deffontaines, O. Lacombe, and J. Angelier (2002), Variations along the strike of the Taiwan thrust belt: Basement control on structural style, wedge geometry and kinematics, in *Geology and Geophysics of an Arc-Continent Collision, Taiwan*, edited by T. B. Byrne and C. S. Liu, *Spec. Pap. Geol. Soc. Am.*, *358*, 293–322.

Nesbitt, B. (1993), Electrical resistivities of crustal fluids, *J. Geophys. Res.*, *98*, 4301–4310, doi:10.1029/92JB02576.

Ng, S. M., J. Angelier, and C. P. Chang (2009), Earthquake cycle in western Taiwan: Insights from historical seismicity, *Geophys. J. Int.*, *178*, 753–774, doi:10.1111/j.1365-246X.2009.04164.x.

Ogawa, Y., et al. (2001), Magnetotelluric imaging of fluids in intraplate earthquake zones, NE Japan back arc, *Geophys. Res. Lett.*, *28*, 3741–3744, doi:10.1029/2001GL013269.

Okaya, D., T. Stern, F. Davey, S. Henrys, and S. Cox (2007), Continent-continent collision at the Pacific/Indo-Australian plate boundary: Background, motivation, and principal results, in *A Continental Plate Boundary: Tectonics of South Island, New Zealand*, *Geophys. Monogr. Ser.*, vol. 175, edited by D. Okaya, T. Stern, and F. Davey, pp. 1–18, AGU, Washington, D. C.

Parkinson, W. D. (1962), The influence of continents and oceans on geomagnetic variations, *Geophys. J. R. Astron. Soc.*, *6*, 411–449.

Rau, R. J., and F. T. Wu (1995), Tomographic imaging of lithospheric structures under Taiwan, *Earth Planet. Sci. Lett.*, *133*, 517–532, doi:10.1016/0012-821X(95)00076-O.

Rodi, W., and R. L. Mackie (2001), Nonlinear conjugate gradients algorithm for 2-D Magnetotelluric inversion, *Geophysics*, *66*, 174–187, doi:10.1190/1.1444893.

Rosenberg, C. L., and M. R. Handy (2005), Experimental deformation of partially melted granite revisited: Implications for the continental crust, *J. Metamorph. Geol.*, *23*, 19–28, doi:10.1111/j.1525-1314.2005.00555.x.

Shyu, J. B. H., K. Sieh, Y. G. Chen, and C. S. Liu (2005), Neotectonic architecture of Taiwan and its implications for future large earthquakes, *J. Geophys. Res.*, *110*, B08402, doi:10.1029/2004JB003251.

Simpson, F., and K. Bahr (2005), *Practical Magnetotellurics*, Cambridge Univ. Press, Cambridge, U. K., doi:10.1017/CBO9780511614095.

Siripunvaraporn, W., G. Egbert, Y. Lenbury, and M. Uyeshima (2005), Three-dimensional magnetotelluric inversion: Data-space method, *Phys. Earth Planet. Inter.*, *150*, 3–14, doi:10.1016/j.pepi.2004.08.023.

Song, T. R. A., and K. F. Ma (2002), Estimation of thermal structure of a young orogenic belt according to a model of whole-crust thickening, in *Geology and Geophysics of an Arc-Continent Collision, Taiwan*, edited by T. B. Byrne and C. S. Liu, *Spec. Pap. Geol. Soc. Am.*, *358*, 121–136.

Soyer, W., and M. J. Unsworth (2006), Deep electrical structure of the northern Cascadia (British Columbia, Canada) subduction zone: Implications for the distribution of fluids, *Geology*, *34*, 53–56, doi:10.1130/G21951.1.

Suppe, J. (1980), Imbricated structure of western foothills belt, south-central Taiwan, *Pet. Geol. Taiwan*, *17*, 1–16.

Suppe, J. (1981), Mechanics of mountain building and metamorphism in Taiwan, *Mem. Geol. Soc. China*, *4*, 67–89.

Suppe, J. (1984), Kinematics of arc-continent collision, flipping of subduction, and back-arc spreading near Taiwan, *Mem. Geol. Soc. China*, *6*, 21–33.

Suppe, J. (1987), The active Taiwan mountain belt, in *Anatomy of Mountain Chains*, edited by J. P. Shear and J. Rogers, pp. 277–293, Princeton Univ. Press, Princeton, N. J.

Teng, L. S. (1990), Geotectonic evolution of late Cenozoic arc-continent collision in Taiwan, *Tectonophysics*, *183*, 57–76, doi:10.1016/0040-1951(90)90188-E.

Teng, L. S. (1996), Extensional collapse of the northern Taiwan mountain belt, *Geology*, *24*, 949–952, doi:10.1130/0091-7613(1996)024<0949:ECOTNT>2.3.CO;2.

Tillman, K. S., and T. B. Byrne (1995), Kinematic analysis of the Taiwan slate belt, *Tectonics*, *14*, 322–341, doi:10.1029/94TC02451.

Tsai, Y. B., Y. M. Hsiung, H. B. Liaw, H. P. Lueng, T. H. Yao, and Y. T. Yeh (1974), A Seismic refraction study of eastern Taiwan, *Pet. Geol. Taiwan*, *11*, 115–182.

Tullis, J., A. Yund, and J. Farver (1996), Deformation-enhanced fluid distribution in feldspar aggregates and implications for ductile shear zones, *Geology*, *24*, 63–66, doi:10.1130/0091-7613(1996)024<0063:DEFDIF>2.3.CO;2.

Türkoğlu, E., M. J. Unsworth, and D. Pana (2009), Deep electrical structure of northern Alberta (Canada): Implications for diamond exploration, *Can. J. Earth Sci.*, *46*, 139–154, doi:10.1139/E09-009.

Twiss, R. J., and E. M. Moores (2007), *Structural Geology*, 2nd ed., Freeman and Company, New York.

Unsworth, M. J. (1999), Magnetotellurics, in *McGraw-Hill 2000 Yearbook of Science and Technology*, pp. 240–242, McGraw-Hill, New York.

Upton, P., D. Craw, B. Yu, and Y.-G. Chen (2011), A comparison of orogenic fluid flow, in *Geology of the Earthquake Source: A Volume in Honour of Rick Sibson*, edited by A. Fagereng, V. Toy, and J. V. Rowland, *Geol. Soc. Spec. Publ.*, *359*, 249–265, doi:10.1144/SP359.14.

Vanyan, L., and A. O. Gliko (1999), Seismic and electromagnetic evidence of dehydration as a free water source in the reactivated crust, *Geophys. J. Int.*, *137*, 159–162, doi:10.1046/j.1365-246x.1999.00767.x.

Wannamaker, P. E. (1999), Affordable magnetotellurics: Interpretation in natural environments, in *Three-Dimensional Electromagnetics*, *Geophys. Dev. Ser.*, vol. 7, edited by M. Oristaglio and B. Spies, pp. 349–374, Soc. of Explor. Geophys., Tulsa, Okla., doi:10.1190/1.9781560802154.ch22.

Wannamaker, P. E. (2000), Comment on "The petrologic case for a dry lower crust" by B. W. D. Yardley and J. W. Valley, *J. Geophys. Res.*, *105*, 6057–6064, doi:10.1029/1999JB900324.

Wannamaker, P. E., G. R. Jiracek, J. A. Stodt, T. G. Caldwell, V. M. Gonzalez, J. D. McKnight, and A. D. Porter (2002), Fluid generation and pathways beneath an active compressional orogen, the New Zealand Southern Alps, inferred from magnetotelluric data, *J. Geophys. Res.*, *107*(B6), 2117, doi:10.1029/2001JB000186.

Wannamaker, P. E., et al. (2008), Lithospheric dismemberment and magmatic processes of the Great Basin-Colorado Plateau transition, Utah, implied form Magnetotellurics, *Geochem. Geophys. Geosyst.*, *9*, Q05019, doi:10.1029/2007GC001886.

Wannamaker, P. E., T. G. Caldwell, G. R. Jiracek, V. Maris, G. J. Hill, Y. Ogawa, H. M. Bibby, S. L. Bennie, and W. Heise (2009), Fluid and deformation regime of an advancing subduction system at Marlborough New Zealand, *Nature*, *460*, 733–736, doi:10.1038/nature08204.

Watson, E. B., and J. M. Brenan (1987), Fluids in the lithosphere, 1. Experimentally determined wetting characteristics of CO_2-H_2O fluids and their implications for fluid transport, host rock physical properties, and fluid inclusion formation, *Earth Planet. Sci. Lett.*, *85*, 497–515, doi:10.1016/0012-821X(87)90144-0.

Watson, E. B., J. M. Brenan, and D. R. Baker (1990), Distribution of fluids in the continental mantle, in *Continental Mantle*, edited by M. A. Menzies, pp. 111–125, Clarendon, Oxford, U. K.

Willett, S. D., D. Fisher, C. Fuller, E. C. Yeh, and C. Y. Lu (2003), Erosion rates and orogenic-wedge kinematics in Taiwan inferred from fission track thermochronometry, *Geology*, *31*, 945–948, doi:10.1130/G19702.1.

Wu, F. T., R. Rau, and D. Slazberg (1997), Taiwan orogeny: Thin-skinned or Lithospheric collision, *Tectonophysics*, *274*, 191–220, doi:10.1016/S0040-1951(96)00304-6.

Wu, F. T., C. S. Chang, and Y. M. Wu (2004), Precisely relocated hypocenters, focal mechanisms and active orogeny in central Taiwan, in *Aspects of the Tectonic Evolution of China*, edited by J. Malpas et al., *Geol. Soc. Spec. Publ.*, *226*, 333–354.

Wu, F. T., W. T. Liang, J. C. Lee, H. Benz, and A. Villasenor (2009), A model for the termination of the Ryukyu subduction zone against Taiwan: A junction of collision, subduction/separation, and subduction boundaries, *J. Geophys. Res.*, *114*, B07404, doi:10.1029/2008JB005950.

Wu, Y. M., C. H. Chang, L. Zhao, T. L. Teng, and M. Nakamura (2008), A comprehensive relocation of earthquakes in Taiwan from 1991 to 2005, *Bull. Seismol. Soc. Am.*, *98*, 1471–1481, doi:10.1785/0120070166.

Yen, H. Y., Y. H. Yeh, and F. T. Wu (1998), Two-dimensional crustal structures of Taiwan from gravity data, *Tectonics*, *17*, 104–111, doi:10.1029/97TC02697.

Yu, S. B., and L. C. Kuo (2001), Present-day crustal motion along the Longitudinal Valley Fault, eastern Taiwan, *Tectonophysics*, *333*, 199–217, doi:10.1016/S0040-1951(00)00275-4.

Yu, S. B., H. Y. Chen, and L. C. Kuo (1997), Velocity field of GPS stations in the Taiwan area, *Tectonophysics*, *274*, 41–59, doi:10.1016/S0040-1951(96)00297-1.

Yu, S. B., L. C. Kuo, R. S. Punongbayan, and E. G. Ramos (1999), GPS observation of crustal deformation in the Taiwan-Luzon region, *Geophys. Res. Lett.*, *26*, 923–926, doi:10.1029/1999GL900148.

E. A. Bertrand and G. J. Hill, GNS Science, 1 Fairway Dr., Avalon, Lower Hutt 5010, New Zealand. (t.bertrand@gns.cri.nz)

C.-C. Chen, C.-S. Chen, and H.-L. Hsu, Institute of Geophysics, National Central University, Jhongli 32001, Taiwan.

C.-W. Chiang, Department of Geosciences, National Taiwan University, Taipei 10617, Taiwan.

E. Türkoğlu, Quantec Geoscience, 146 Sparks Ave., Toronto, ON M2H 2S4, Canada.

M. J. Unsworth, Department of Physics, University of Alberta, Edmonton, AB T6G 2R3, Canada.

F. T. Wu, Department of Geological Sciences and Environmental Studies, State University of New York at Binghamton, Binghamton, NY 13902-6000, USA.